6TH INTERNATIONAL CONFERENCE ON DAM ENGINEERING
C.Pina, E.Portela, J.Gomes (ed.)
Lisbon, Portugal, February 15-17, 2011

ENVIRONMENTAL THERMAL ACTIONS - THERMAL ANALYSIS OF ALTO LINDOSO DAM

Noemí A. Schclar Leitão*

* Laboratório Nacional de Engenharia Civil (LNEC)
Av. do Brasil, 101, 1700-066 Lisboa, Portugal
e-mail: nschclar@lnec.pt, webpage: http://www.lnec.pt

Keywords: Concrete Dams, Finite Element Method, Heat Transfer, Environmental Actions

Abstract. *In this work the finite element implementation of thermal analysis of concrete dams is described. The different temperature boundary conditions are properly represented. For the exposed face of the dam both convection/radiation heat transfer and solar radiation are implemented. The model is validated by calculating the response of a concrete arch dam and comparing the results of the monitoring system values.*

1 INTRODUCTION

The study of temperature monitoring and thermal analysis began at the "Centro de Estudos de Engenharia Civil", predecessor of the "Laboratório Nacional de Engenahria Civil" (LNEC), in the late 1940's when construction of large dams was initiated in Portugal[1].

Based on that experience, and in an attempt to address the problem within the dam designers community, a Specialist Thesis was presented by Silveira[2] in 1961 summing up the main concepts of heat transfer, thermal stresses and thermal properties determination that were available at that time. Particular emphasis was laid on climatic factors, among which air and water temperatures and solar radiation were studied in detail. The main drawback was that the closed form solutions presented in that work were restricted to regular geometries.

Parallel to his work, there was also an effort to develop experimental techniques for the characterization of the thermal and thermo-mechanical properties of the materials, particularly the diffusivity and thermal expansion coefficient determination[3].

In an attempt to better understand how the temperature changes affected the state of stress in concrete dams, the research in the 1960's focused in the use of reduced physical models[4, 5]. The developed technique allowed the application of uniform temperature variation, temperature gradients in steady state between the two faces of the dam and transient regimes resulting from thermal shock or thermal sinusoidal wave corresponding to periods of one year[6]. Despite the great importance of the results obtained by these experimental studies, their limitations in reproducing the thermal loads and the material behaviour were considered reasons enough to abandoning this type of studies.

Following the world trend, the 1970's was characterized by the development of computer-based structural analysis, and by 1980's this new approach was extended for the thermal analysis of concrete dams[7]. The implemented finite element program allowed representing the real three dimensional geometry of the dams, but adiabatic or imposed temperatures were the only boundary conditions available in those days.

By the 1990's, the computer revolution and the growing capabilities of the commercial software made possible a more realistic representation of thermal problems. Convective and radiative boundaries conditions and the construction sequence simulation were easy to model[8].

As it is well known, commercial general-purpose numerical analysis packages have a large number of built in features, solid modelling capabilities and a graphical user interface, so the user does not need to spend time and energy developing the capabilities that they need for his application. However, to write a customized subroutine to commercial software is not always an easy task. In the case when we are focused in the resolution of a small number of well-defined applications the use of an in-house code can be worthwhile. For this reason a new finite element code was recently developed to take into account the specificities of concrete dams analysis. The new code allows the simulation of the environmental thermal conditions (temperature of the reservoir, air temperature and solar radiation), the heat of hydration (both approaches, adiabatic and thermally-activated process, were implemented) and the dam construction schedule.

To take advantage of the simplicity of an in-house code instead of a monolithic program it was decided to write different programs addressing the construction stage (a linear version for the adiabatic hydration process and a non linear one for the thermally-activated process) and the exploration stage. All the programs access a common subroutine library. The programs are written in FORTRAN 90 using the structured programming style proposed by Smith and Griffiths[9] and its companion library of free subroutines[10].

In this article the code corresponding to the thermal analysis of dams during the exploration stage will be presented. It will be applied in order to compute the temperature field of the Alto Lindoso dam. The validation of these results and the induced displacements will be performed by comparison with the values measured with the monitoring system installed in the dam.

2 THERMAL ANALYSIS ALGORITHM

The transient heat conduction equation for a stationary medium is given by[11]:

$$\frac{\partial}{\partial x}\left[k_x \frac{\partial T}{\partial x}\right]+\frac{\partial}{\partial y}\left[k_y \frac{\partial T}{\partial y}\right]+\frac{\partial}{\partial z}\left[k_z \frac{\partial T}{\partial z}\right]+G=\rho c \frac{\partial T}{\partial t} \tag{1}$$

with the boundary conditions:

$$T=\overline{T} \qquad \text{in } \Gamma_T \tag{2}$$

$$k_x \frac{\partial T}{\partial x} l+k_y \frac{\partial T}{\partial y} m+k_z \frac{\partial T}{\partial z} n+q+h(T-T_a)=0 \qquad \text{in } \Gamma_q \tag{3}$$

and the initial condition:

$$T=T_o \qquad \text{in } \Omega \text{ for } t=t_o \tag{4}$$

where t is the time; T is the temperature; T_a is the air temperature; $\overline{T}$ is the temperature at the boundary Γ_T; T_o is the temperature at time t_o; q is the prescribed flux at the boundary Γ_q; k_x, k_y and k_z are the thermal conductivities; G is the internally generated heat per unit of volume and time; ρ is the material density; c is the specific heat; h is the heat transfer coefficient; and l, m and n are the cosine directors.

In dam engineering, G, Γ_T, Γ_q, $\overline{T}$ and q are associated[12], respectively, to the heat of hydration, the concrete water interface, the surfaces exposed to the air, the reservoir water temperature, and the solar radiation.

The temperature is discretized over space as follow:

$$T(x,y,z,t) = \sum_{i=1}^{m} N_i(x,y,z)\, T_i(t) \tag{5}$$

where N_i are the shape functions, m is the number of nodes in an element and $T_i(t)$ are the time-dependent nodal temperatures.

After applying the Finite Element Method in space and introducing the θ-method for time integration, the resulting fully discretized system of linear algebraic equations can be written as:

$$([\mathbf{C}]+\theta\Delta t[\mathbf{K}])\{\mathbf{T}\}^{n+1} = ([\mathbf{C}]-(1-\theta)\Delta t[\mathbf{K}])\{\mathbf{T}\}^{n} + \Delta t\left(\theta\{\mathbf{f}\}^{n+1} + (1-\theta)\{\mathbf{f}\}^{n}\right) \tag{6}$$

where $[\mathbf{C}]$ is the capacitance matrix, $[\mathbf{K}]$ is the heat stiffness (conduction and convection) matrix and $\{\mathbf{f}\}$ is the total load heat vector:

$$\{\mathbf{f}\} = \int_{\Omega} G[\mathbf{N}]^{\mathrm{T}}\, d\Omega - \int_{\Gamma_q} q[\mathbf{N}]^{\mathrm{T}}\, d\Gamma_q + \int_{\Gamma_q} hT_a[\mathbf{N}]^{\mathrm{T}}\, d\Gamma_q \tag{7}$$

where the first integral takes into account the internal heat generation, the second integral takes into account the prescribed heat flow and the third integral takes into account the convection heat transfer.

2.1 Time dependent temperatures

The main difference with other heat transfer applications is that the temperatures $\overline{T}$ and T_a are not functions of the variable t but of the time of the day and the time of the year. To implement this dependence the concept of the Julian day is used.

According to the system of numbering days called Julian day numbers, used by astronomers, the temporal sequence of days is mapped onto the sequence of integers. The starting point is January 1, 4713 BC. This makes it easy to determine the number of days between two dates (just subtract one Julian day number from the other). Julian Days can also be used to tell time; the time of day is expressed as a fraction of a full day, with 12:00 noon (not midnight) as the zero point. The algorithm to convert from Gregorian calendar date to Julian day can be found in any book on astronomy.

In this way, the user indicates the period to be analyzed by just writing the initial and final date in the Gregorian calendar. During execution, a subroutine makes the conversion to the correspondent Julian day.

2.1 Solar radiation

In the case of the solar radiation, the difference is not only that the prescribed flux depends on the time of the day and the time of the year, but also it varies with the orientation of the surface.

The measurement of solar radiation is generally accomplished through global irradiance incident on a horizontal surface (oriented towards the zenith) I_h. For an arbitrary orientated surface, the solar radiation takes the form:

$$I_\alpha = \frac{I_h}{\cos Z}\cos\alpha \tag{8}$$

where Z is the solar elevation and α is the incidence angle.

The solar elevation Z is the angle formed by the vertical line of the place (zenith) and the line connecting to the sun. It can be formulated in terms of the sun's declination δ, the earth's latitude ϕ, and the hour angle of the sun t:

$$\cos Z = \sin\phi \sin\delta + \cos\phi\cos\delta\cos t \tag{9}$$

where the declination of the sun can be represented by the Spencer's formula given by13:

$$\begin{aligned}\delta &= 0{,}006918 - 0{,}399912\cos(\gamma) + 0{,}070257\ \sin(\gamma)\\ &- 0{,}006758\cos(2\gamma) + 0{,}000907\ \sin(2\gamma)\\ &- 0{,}002697\cos(3\gamma) + 0{,}00148\ \sin(3\gamma)\end{aligned} \tag{10}$$

where γ is the date expressed as an angle ($\gamma = \frac{2\pi}{365}(N-1)$; N = day number ranging from 1 on January 1st to 365 on December 31st); both δ and γ are in degrees.

The incidence angle α is the angle between the incident solar radiation and the normal to the surface. It can be formulated in terms of the angle of inclination of the surface, relative to the horizontal plane, Y, the sun's declination δ, the earth's latitude ϕ, the hour angle of the sun t and the azimuth β:

$$\cos\alpha = A\sin\delta + B\cos t\cos\delta - C\ \sin t\cos\delta \tag{11}$$

with

$$\begin{aligned}A &= \cos Y\ \sin\phi - \sin Y\cos\phi\cos\beta\\ B &= \cos Y\cos\phi + \sin Y\sin\phi\cos\beta\\ C &= \sin Y\,\mathrm{sen}\beta\end{aligned} \tag{12}$$

When $\cos\alpha < 0$ the solar radiation $I_\alpha = 0$, because in this case there is no incidence of sunlight to the considered surface.

From the computational point of view, the angles Y and β are defined in each integration point by the components of the normal vector $\vec{g}$, represented in Figure 1, given by:

$$g_x = \frac{\partial y}{\partial\xi}\frac{\partial z}{\partial\eta} - \frac{\partial z}{\partial\xi}\frac{\partial y}{\partial\eta};\ g_y = \frac{\partial z}{\partial\xi}\frac{\partial x}{\partial\eta} - \frac{\partial x}{\partial\xi}\frac{\partial z}{\partial\eta};\ g_z = \frac{\partial x}{\partial\xi}\frac{\partial y}{\partial\eta} - \frac{\partial y}{\partial\xi}\frac{\partial x}{\partial\eta} \tag{13}$$

with $\frac{\partial x}{\partial\xi} = \sum\frac{\partial N_m}{\partial\xi}x_m$ and N_i represent the shape functions of the element face.

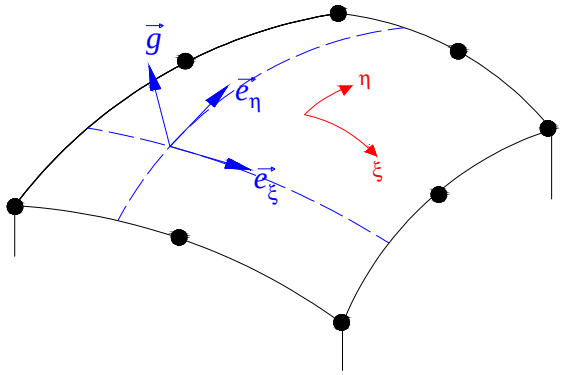

Figure 1: Normal vector $\vec{g}$ on the curved face of a finite element

3 ALTO LINDOSO DAM

Alto Lindoso dam is located in the North of Portugal, a few hundred meters from the Spanish border. It is a double curvature concrete arch dam with a maximum height of 110 m, a thickness of 21 m at the base of the crown cantilever and of 4 m at the crest. The crest length is 297 m. Its latitude is 41° 52' and its axis forms an angle of 52 degrees with the South (Figure 2). The concreting of the dam took place between April 1987 and July 1990. The injection of contraction joints took place between March and May 1991. The first filling of the reservoir began on January 6, 1992, with the water level in the reservoir at elevation 234 m, and ended on April 28, 1994, when the water level reached 338 m elevation.

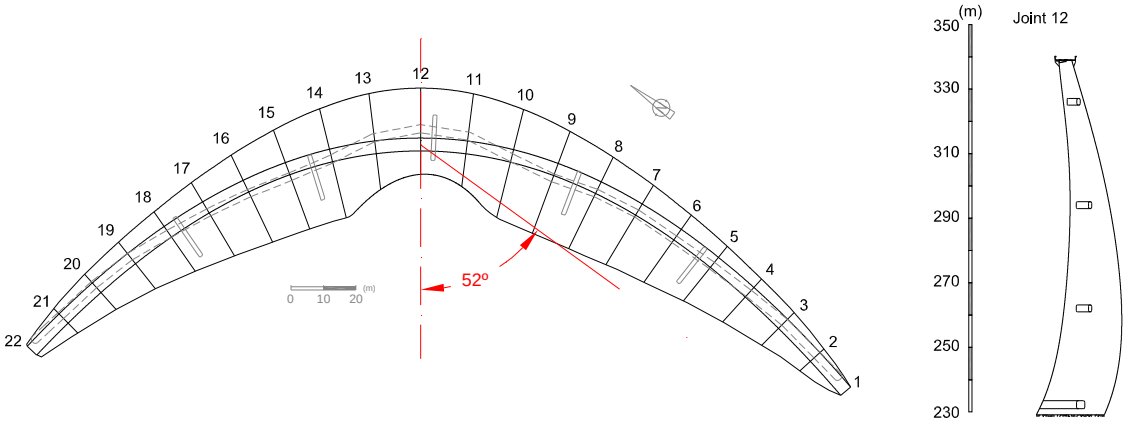

Figure 2: Alto Lindoso dam

About 400 instruments of various types were installed in the dam as part of its monitoring system; they supply continuous information on displacements, deformations, seepage, uplift pressures, and ambient and internal temperatures.

The analysis was carried out using the finite element mesh shown in Figure 3. It is composed of 2022 isoparametric 20-node elements for a total of 10,077 nodes.

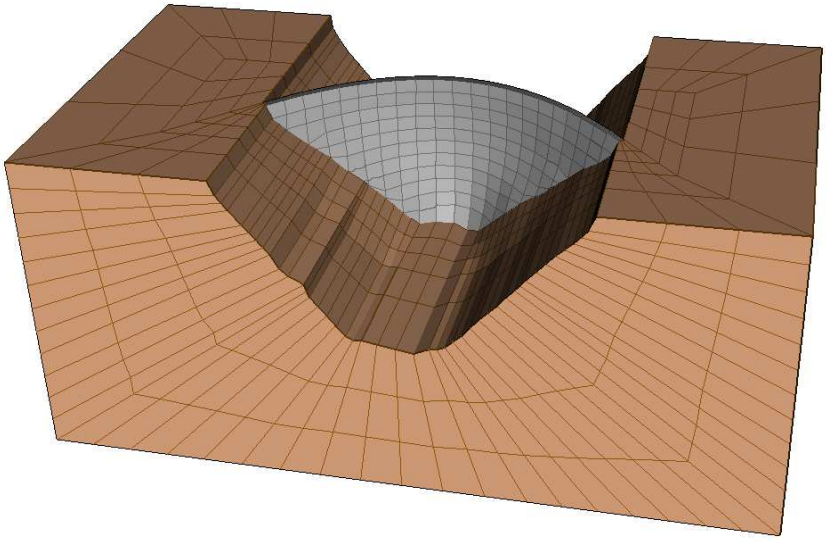

Figure 3: Finite element mesh

The adopted values for the thermal properties of concrete and rock are listed in Table 1.

Parameters	Unit	Value
Specific heat c	[J/(kg K)]	920
Thermal conductivity k_{ii}	[W/(m K)]	2,62
Density ρ	[kg/m^3]	2400
Solar absorptivity a		0,65 (concrete)
		0,00 (rock)
Convection coefficient h_t	[W/(m^{2}K)]	25

Table 1: Thermal properties.

The daily air temperature was represented as the superposition of an average temperature of two harmonic functions, one of annual period and another with a one day period.

$$T(t') = 14.6 + 6.68\cos\left[\frac{2\pi}{365}(t'-24.1)\right] + T_a^d(t')\cos\left[2\pi(t'-0.125)\right] \qquad [^oC] \qquad (14)$$

with

$$2\times T_a^d(t) = A(t) = 9.52 + 2.35\cos\left[\frac{2\pi}{365}(t-1.87)\right] \qquad [^oC] \qquad (15)$$

The calculation of the parameters involved in these functions was done based on the average daily air temperatures registered at the dam site using the least squares method.
The convection coefficient h_c was estimated with the expression given by Silveira:

$$h_c = 0{,}055\frac{k_f}{L}\left(\frac{L\,V\,\rho_f}{\mu_f}\right)^{0,75} \qquad \left[\frac{W}{m^2\,K}\right] \qquad (16)$$

where k_f, ρ_f and μ_f are, respectively, the thermal conductivity, density and absolute viscosity of air, which correspond to the values of 0.026 W/(m K), 1.2 kg/m^3 and 1.8x10^{-5} kg/(m s), V is the average wind speed and L represents the size of the considered flat surface for which Silveira adopted the value of 0.60 m. Regarding the average wind speed a value of

4.5 m/s was adopted, resulting in a convection coefficient h_c of 20 W/(m^2 K). To take into account the radiation heat transfer from the dam to the air, the linearized radiation coefficient h_r was added to the convection coefficient h_c. For the range of temperature values registered in Portugal, Silveira adopted a constant value of $h_c = 5$ W/(m^{2}K).

For the water reservoir temperature the approximation given by Zhu[14] was adopted:

$$T(y,t') = T_m(y) - T_a(y)\cos\left\{\frac{2\pi}{365}\left[t' - t_o(y)\right]\right\} \qquad [^oC] \tag{17}$$

with:

$$T_m(y) = 10.3 + (16.1 - 10.3)\exp(-0.027y) \qquad [^oC] \tag{18}$$

$$T_a(y) = -6.19\exp(-0.0103y) \qquad [^oC] \tag{19}$$

$$t_o(y) = \left[1.87 - 2.00\exp(-0.0708y)\right](365/12) + 24.1 \qquad [\text{days}] \tag{20}$$

where y is the water depth [m] and t' is the time [days]. The calculation of the parameters involved in these functions was done using the temperatures measured in the water concrete interface.

For the determination of the solar radiation the solar radiation function over a horizontal surface given by Silveira was used:

$$I = \frac{I_h}{\cos Z} = 1367\exp\left(-1.13 + 0.96\cos Z\right) \qquad [\text{W/m}^2] \tag{21}$$

In order to illustrate the performance of the solar irradiation computations, Figure 4 shows the computed solar irradiation of the downstream face at 12:49 a.m. and 4:46 p.m. on 18 of February 2009 together with the photo taken at the site.

Although the representation of the shades caused by the surrounded terrain and the geometry of the structure itself were not implemented in the code, as it is recently presented by Feng Jin and co-authors[15], the result can be considered a good approximation of the reality.

Beyond the boundary conditions, the thermal analysis also required the initial temperature field. However, for dams at exploration stage this point is easily solved by assuming an initial estimated value and applying the boundary conditions for a certain period of time until the dam reaches a steady state behaviour[16].

Figure 5 shows the temperatures computed at different points near the crest of the block 15/16, where both faces of the dam are exposed to ambient temperature and solar radiation. Due to the scale used in the representation, the effect of daily temperature variation is reflected as an increased thickness of the annual thermal temperature wave. The points represent the monitored temperatures in the thermometers T13 and T16, located, respectively, downstream and upstream of the dam, and in the Carlson extensometer G7 and G8, located at 1 m of the downstream and upstream face, respectively. It is to note the wider thickness of the downstream temperature wave (thermometer T13) in comparison with upstream one (thermometer T16) due to the influence of the solar radiation in the downstream face.

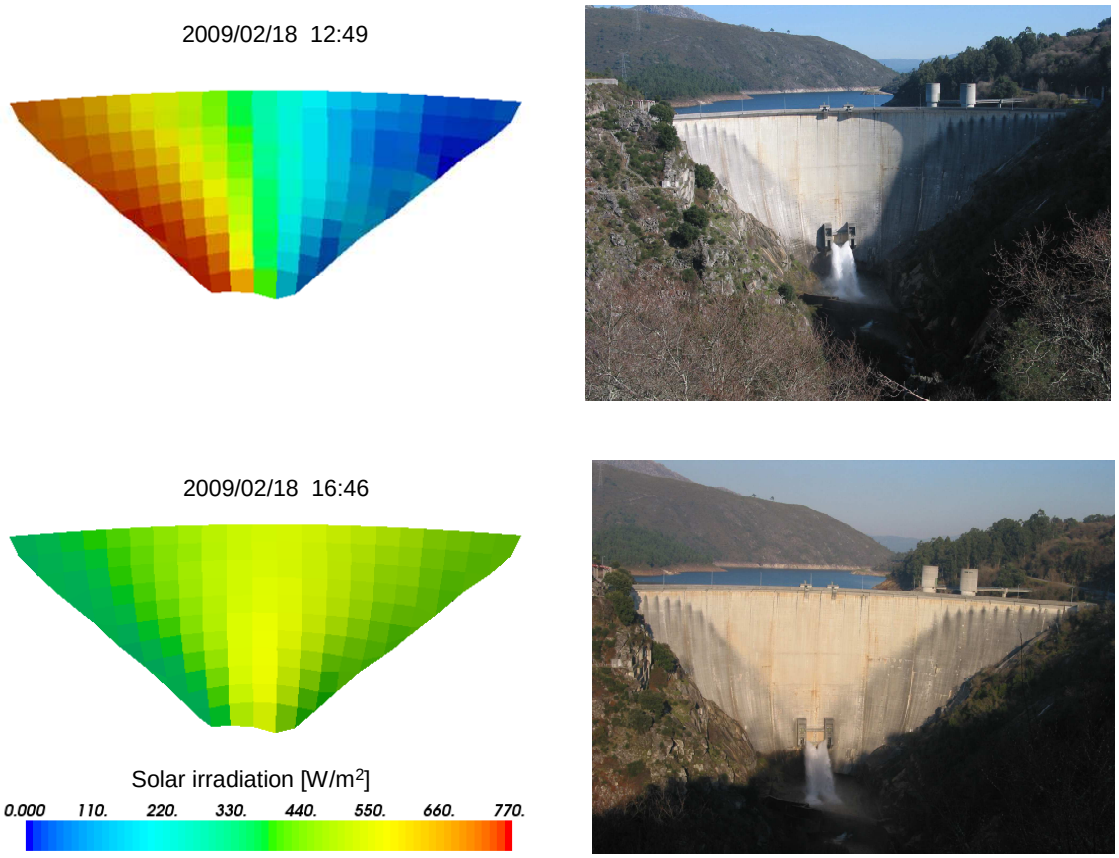

Figure 4: Solar irradiation

The exposure to the solar radiation also explains the crowding of the measured points at the bottom of the temperature annual wave in the downstream face (thermometer T13) which is explained by the fact that the temperatures are always recorded during the morning, when the face is less exposed to the incidence of sunlight

After the annual temperature variation of the dam was computed, a linear mechanical analysis was carried out. Table 2 gives the mechanical properties adopted for the computation[17].

Parameter	Unit	Value
Concrete		
Elastic modulus E_b	[GPa]	32
Poisson's ratio ν_b		0,2
Coefficient of thermal expansion α_b	$°C^{-1}$	0,95 x 10^{-5}
Rock mass		
Elastic modulus E_f	[GPa]	15; 30 and 40 (see Fig. 6)
Poisson's ratio ν_f		0,2
Coefficient of thermal expansion α_f	$°C^{-1}$	0,85 x 10^{-5}

Table 2: Mechanical properties.

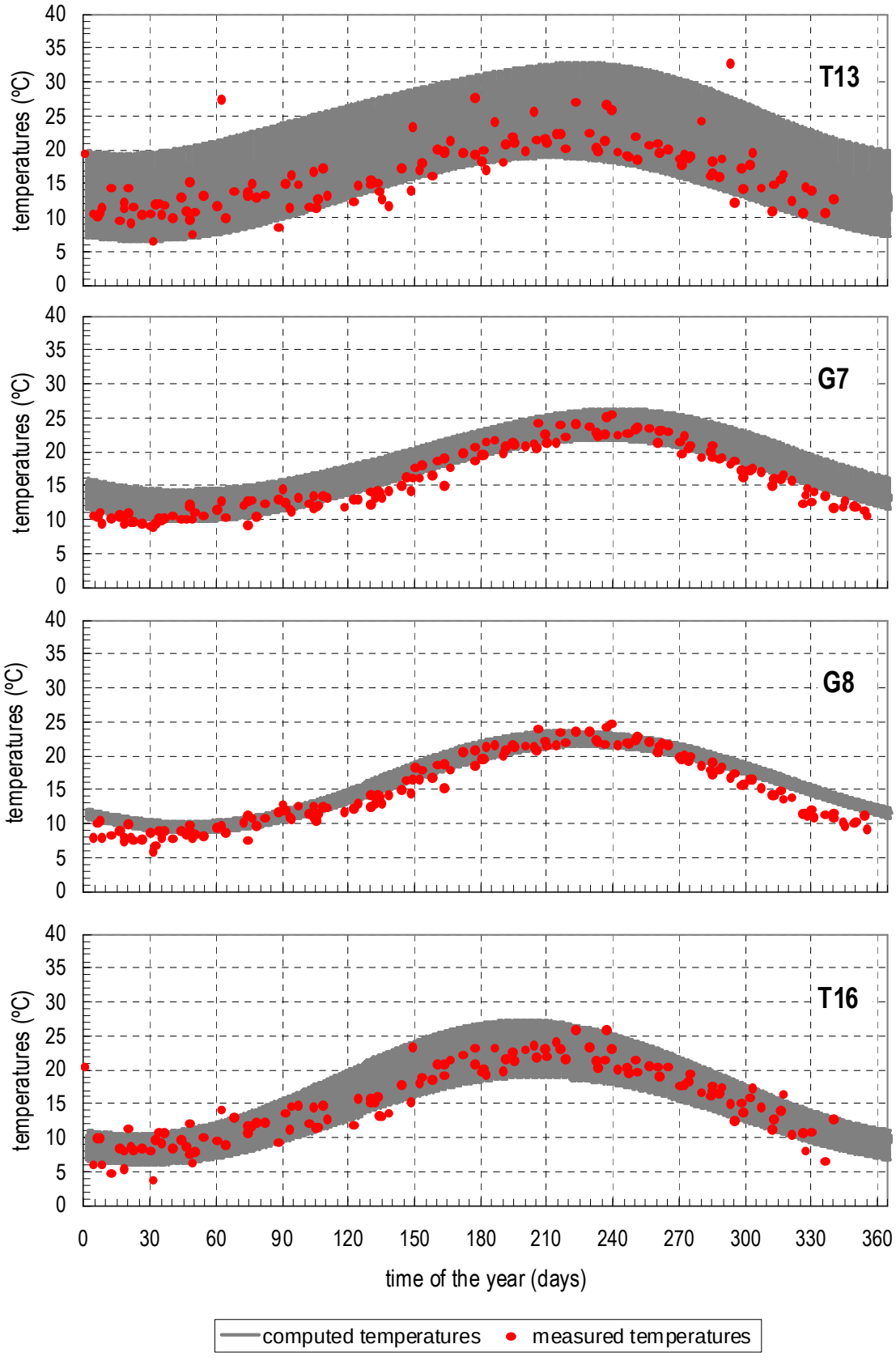

Figure 5: Annual temperature distributions in block 15/16 near the crest

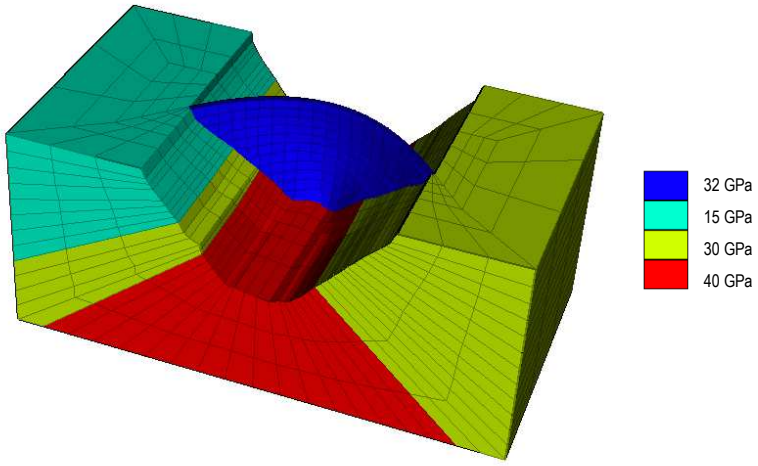

Figure 6: Elastic modulus

In order to validate these results, it was necessary to decompose the observed displacements into their three mains components, that is, the hydrostatic pressure component, the thermal component, and the irreversible component due to the non-elastic behavior of the dam, using a statistical method.

The elastic analysis was carried out for the temperature decrease obtained between the temperatures computed in August and February.

In Figure 7 the computed horizontal radial displacement are compared with the measured displacements by the pendulums located at blocks 5/6, 8/9, 11/12, 14/15 and 17/18.

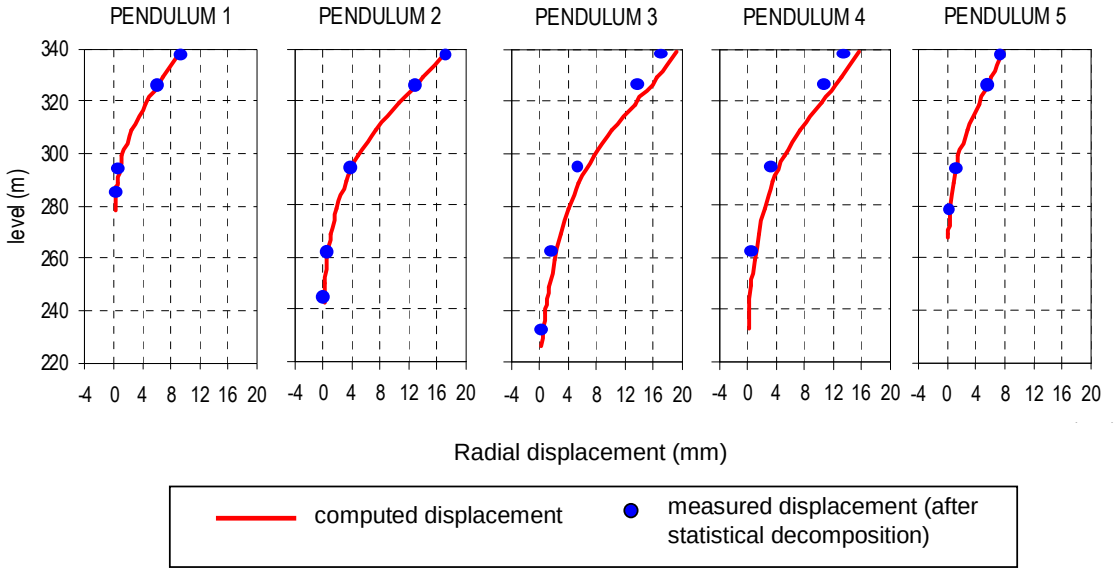

Figure 7: Comparison between computed and measured displacement

4 CONCLUSIONS

In this work a method for thermal analysis of concrete dams has been formulated and numerically validated. The proposed model takes account of the different types of

temperature boundary conditions: concrete-water interface, concrete-air interface and concrete-rock foundation interface. For the concrete-air interface both convection/radiation heat transfer and solar radiation was considered. The model was applied to Alto Lindoso dam. A good agreement between numerically calculated and measured quantities was achieved.

ACKNOWLEDGMENT

Thanks are due to EDP – Gestão da Produção de Energia, S.A. for permission to publish data relative to Alto Lindoso dam.

REFERENCES

[1] M. Rocha, J. Serafim and A. Silveira, "Observation of dams. Methods and apparatus used in Portugal", *RILEM - Symposium on the observation of structures*, pp. 560-587, Lisbon, Portugal (1955).

[2] A. Silveira, *Temperatures variations in dams*, (in portuguess), LNEC Memória nº 177, Lisbon, Portugal (1961).

[3] M. Rocha and J.L: Serafim, "Determination of thermal stresses in arch dams by means of models", *VI Congress on Large Dams*, New York, USA (1958).

[4] M. Rocha, J.L. Serafim, A. Cruz and A. Cobeira, "Determination of thermal stresses in arch dams by means of models", *bulletim RILEM*, nº 10, Paris, France (1961).

[5] M. Rocha and A. Silveira, *The use of models to determine temperature stresses in concrete dams*, Thechnical Paper nº 230, LNEC, Lisbon, Portugal (1964).

[6] M. Rocha and A. Silveira, "Determination of thermal stresses in concrete dams by means of model tests", *ACI SP24: Models of concrete structures*, pp. 387-406, USA (1970).

[7] M. Teles, *Thermal behaviour of concrte dams*, (in portuguess), PhD Thesis, University of Porto, Porto, Portugal (1986).

[8] A.T. Castro, T. Santana and N.S. Leitão, "Thermal analysis of a RCC dam during construction uding FLAC", *7th Benchmark Workshp on Numerical Analysis od Dams*, Bucharest, Romania (2003)

[9] I.M. Smith and D.V. Griffiths, *Programming the Finite Element Method*, 4th edition. Wiley, U.K. (2006).

[10] www.mines.edu/fs_home/vgriffit/4th_ed/Software.

[11] R. Lewis, P. Nithiarasu and K. Seetharamu, *Fundamentals of the Finite Element Method for Heat and Fluid Flow*. Wiley, U.K. (2004).

[12] F. Sheibany and M. Ghaemian, "Effects of environmental action on thermal stress analysis of Karaj concrete arch dam", *Journal of Enineering Mechanics*, Vol. 132, No. 5, pp. 532-544. ASCE (2006).

[13] J. Almorox and C. Hontoria, "Global solar radiation estimation using sunshine duration in Spain", *Energy Conversion and Management*, 45, pp. 1529–1535 (2004).

[14] B. Zhu, "Prediction of water temperature in deep reservoirs". *Dam Engineering*, VIII, Issue 1, pp. 13–25 (1997).

[15] F. Jin, Z. Chen, J. Wang and J. Yang, "Practical procedure for predicting non-unifrom temperature on the exposed face of arch dams", *Applied Thermal Engineering* 30, pp. 2146-2156 (2010).

[16] P. Zhang, *Cracking and failure of hydroelectric engineering structures due to thermal loads*. PhD Thesis, University of Manitoba, Canada (1998).

[17] LNEC, *Observation of Alto Lindoso dam during the first infilling of the reservoir*, (in portuguess), Relatório LNEC 208/92 – NO, Lisbon, Portugal (1992).